

# Electrolyte Electroreflectance and Photoelectrochemical Topological Investigation of Polycrystalline CuInSe<sub>2</sub> Electrodes by Scanning Light-Spot Optical Microscopy

G. Razzini and L. Peraldo Bicelli\*

Centro di Studio sui Processi Elettrodici del CNR, Dipartimento di Chimica Fisica Applicata del Politecnico, Piazza L. Da Vinci, 32, 20133 Milano, Italy

B. Scrosati\*

Università "La Sapienza," Dipartimento di Chimica, Piazzale Aldo Moro, 5, 00185 Roma, Italy

P. Salvador and M. Pujadas

Instituto de Catalisis y Petroleoquímica, CSIC, Serrano 119, 28006 Madrid, Spain

F. Decker

Instituto de Física, UNICAMP, 13081 Campinas, S.P., Brazil

## ABSTRACT

Using a light-spot technique which allows electro-optical and photoelectrochemical measurements while observing the electrode surface under "a reflex microscope," the inhomogeneities and surface defects of polycrystalline CuInSe<sub>2</sub> electrodes were studied. Lead electrodeposition on the semiconductor surface was performed and it was shown to occur preferentially on localized surface regions. The configuration of the electrode deposit resembled closely the electrolyte electroreflectance map obtained from a systematic topological investigation. In fact, the intensity of the  $\Delta R/R$  signal was higher in the regions where lead electrodeposition took place and vice versa. These results revealed that low-doped (high resistivity) domains exist on the surface of the n-type chalcogenide. Electroreduction of the semiconductor surface at potentials near flatband occurred at the less resistive area where bands unpinning was observed by electrolyte electroreflectance. This was not the case for the low-doped domains of high resistivity where the bandedges remained pinned. Light-spot photoelectrochemical measurements with both monochromatic and white light illumination confirmed the electro-optical results.

CuInSe<sub>2</sub>-based photovoltaic as well as photoelectrochemical (PEC) solar cells have shown impressive output stability and high conversion efficiency. Stable PEC cells can be made using n-CuInSe<sub>2</sub> photoanodes in contact with an aqueous polyiodide electrolyte (1-13). Polycrystalline n-CuInSe<sub>2</sub> electrodes have shown solar energy conversion efficiencies up to 12% in this electrolyte (11). Since such polycrystalline samples are characterized by a very large grain size (up to 1-2 mm), donor concentration inhomogeneities as well as segregation phenomena at grain boundaries could easily be resolved by means of an optical technique using radiation in the visible or in the near IR range. A "reflex microscope" provides an excellent optical system to observe the semiconductor electrode surface at the same time when *in situ* electroreflectance (EER) and PEC experiments are performed. Such a system was previously employed to study the PEC behavior of MoSe<sub>2</sub> photoanodes (14). The same system was used in the present work to analyze the EER and photocurrent signal from different surface areas of n-CuInSe<sub>2</sub> electrodes. This helped us to understand the influence of the semiconductor inhomogeneities on the PEC cell performance. In addition, metal electrodeposition revealed the existence of surface inhomogeneities and defects in agreement with the information obtained from the topological investigation by optical microscopy.

EER is a well-known spectroscopic technique, particularly suitable for the *in situ* study of the semiconductor-electrolyte interface when the surface chemistry of the semiconductor electrode is under control (15). Provided that stabilizing electrolytes and adequate potentials are used, EER is a nondestructive technique allowing not only the measurement of the semiconductor direct bandgap energy and the flatband potential,  $V_{FB}$  (16), but also the detection of rapid  $V_{FB}$  shifts associated with chemical and/or PEC reactions occurring at the semiconductor-electrolyte interface (17, 18).

\* Electrochemical Society Active Member.

Topological investigations using EER have been reported with semiconductors inhomogeneously doped (19, 20), and laser scanning techniques have been adapted to detect local variations in the quantum efficiency of semiconductor-electrolyte junctions (21).

Compared with laser scanning, the optical microscopy technique gives the advantage of simultaneously observing the electrode surface. This was shown to be very helpful in detecting the sites of hydrogen evolution and of iodine production during hydroiodic acid photodecomposition on layer-type transition metal dichalcogenides (22). Again, it turned out to be very useful in the present work for identifying surface areas with different PEC activity. Moreover, grain boundaries and localized defects were shown up very clearly on the surface of the polycrystalline CuInSe<sub>2</sub> samples, so that it was easy to go back with the light beam to the same region, though the electrode had to be removed from the cell in order to undergo different surface treatments.

## Experimental

Polycrystalline samples of n-CuInSe<sub>2</sub> were prepared by direct synthesis from the elements at 1050°C and kindly provided by Dr. L. Zanotti of the MASPEC Laboratories in Parma.

Slices having a surface area of 0.2-0.3 cm<sup>2</sup> were back-contacted with an indium and silver paste, mounted on a Teflon holder and sealed with an epoxy resin. The crystals were polished to 0.2 μm finish and etched with a Br<sub>2</sub>/methanol (2%) solution for 10-20s.

The electrodes so prepared were mounted in a three-electrode cell. The semiconductor surface was parallel to the optical window at the bottom of the same cell at a distance of about 1 mm. A saturated calomel electrode (SCE) was used as reference electrode. The electrolyte was mainly an aqueous solution of 2M KI and 0.01M I<sub>2</sub>. All the chemicals were reagent grade and the solutions were prepared with distilled water.

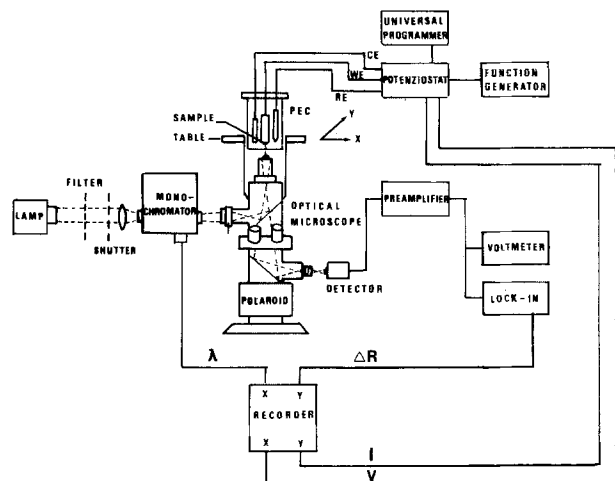


Fig. 1. Experimental setup for *in situ* measurement of the electroreflectance spectra and the photoelectrochemical performance of a semiconductor/electrolyte junction.

The light source in the optoelectronic measurements was a 100W tungsten lamp. Unpolarized light from an Applied Photophysics  $f/3.4$  monochromator was focused on the entrance of the optical path of the Reichert  $\text{MeF}_2$  microscope (Fig. 1).

An  $\times 15$  objective with a working distance of about 5 mm was employed to obtain a light spot of about  $400 \mu\text{m}$ . Changing the objective type, light-spots of about  $100 \mu\text{m}$  could even be obtained.

The PEC cell was placed on the specimen supporting table of the microscope so that the light from the objective could fall perpendicularly on the semiconductor surface and be reflected along the same direction. In order to observe *in situ* the overall semiconductor surface and to perform EER and PEC measurements point by point, we moved the experimental cell along the X and Y direction by means of the specimen supporting table.

The light reflected from the semiconductor surface was detected by a Photodine 775 germanium photodiode utilizing the optical path foreseen for the lateral adaptable camera. The specimen micrographs were taken with a polaroid camera on the front side of the microscope.

The optical reflectance,  $R$ , and the modulated reflectance signal,  $\Delta R$ , were simultaneously detected by a Keithley 169 digital voltmeter via a preamplifier and via a preamplifier

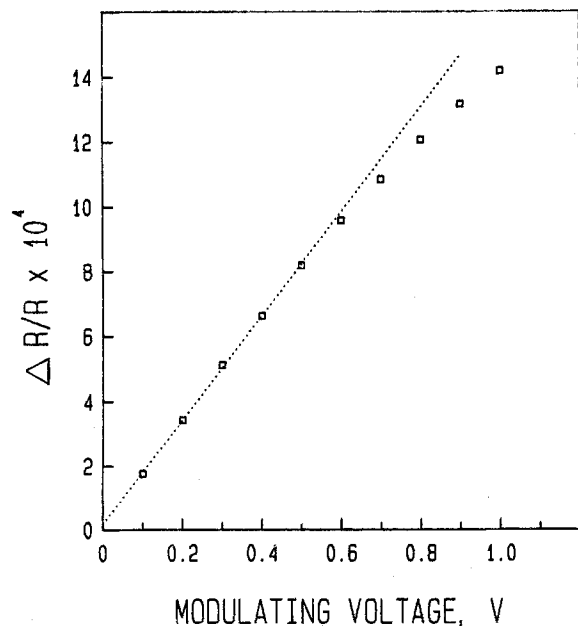


Fig. 2. Electroreflectance response at  $\lambda = 1215 \text{ nm}$  of polycrystalline  $n\text{-CuInSe}_2$  electrodes polarized at  $V_{dc} = 0.0\text{V}$  vs. SCE in the aqueous polyiodide solution as a function of the  $V_{ac}$  bias.

plus a PAR 128 A lock-in amplifier, respectively. As the  $R$  signal was practically constant over the explored wavelength, only the modulated reflectance signal  $R$  was sent to the HP 7040A X-Y recorder to obtain the EER spectrum.

Modulation was accomplished with a 200 Hz sinusoidal modulating signal of 0.3V peak-to-peak amplitude from an HP 3312 A function generator. To polarize the working electrode at the different voltage values, a 553 Amel potentiostat and a 567 Amel universal programmer were used.

The measurements were performed in the low-field modulating regime. In order to verify that these conditions were satisfied, we measured the intensity of the EER peak as a function of the modulating voltage ( $V_{ac}$ ) for a constant dc bias ( $V_{dc}$ ). As shown in Fig. 2, a linear relationship is obtained up to 0.5V which is our operating range.

## Results and Discussion

Several specimens of polycrystalline  $\text{CuInSe}_2$  (nominally, n-type) have been examined following our *in situ* technique which allows the simultaneous optical microscopy observation of the semiconductor surface and the evaluation of its electro-optical and PEC properties. Finally, we selected two typical samples for the further development of the research. Such samples, in the following called S1 and S2, were examined under the optical microscope after the potentiostatic deposition of lead on their surface. We chose this metal owing to the favorable potential of the  $\text{Pb}/\text{Pb}^{2+}$  redox couple ( $E^\circ = -0.37\text{V}$  vs. SCE) which is less negative than the flatband potential of  $\text{CuInSe}_2$  ( $-0.55\text{V}$  vs. SCE) (15).

As shown in Fig. 3b and 4b, lead electrodeposition occurred preferentially on some areas of the electrode surface (area A, upper part of Fig. 3a) and clearly decorated the grain boundaries, as is particularly evident in the lower

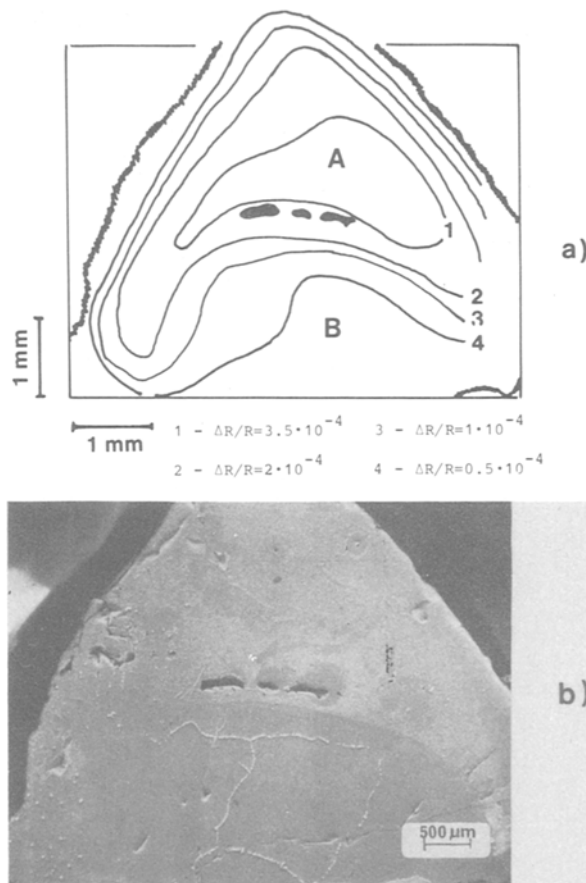


Fig. 3. (a) Map of the  $\Delta R/R$  response of the pristine surface of the  $\text{CuInSe}_2$  sample S1 in the aqueous polyiodide solution under illumination with a 1216 nm light spot ( $V_{ac} = 0.3\text{V}$  peak-to-peak,  $f = 200 \text{ Hz}$ ). The electrode was dc biased at  $0\text{V}$  vs. SCE. The curves connect the points showing the same  $\Delta R/R$  value. (b) Micrograph of the surface of the same sample S1 after lead electrodeposition at  $-0.5\text{V}$  vs. SCE for 3 min in a  $1\text{M PbCl}_2$  aqueous solution.

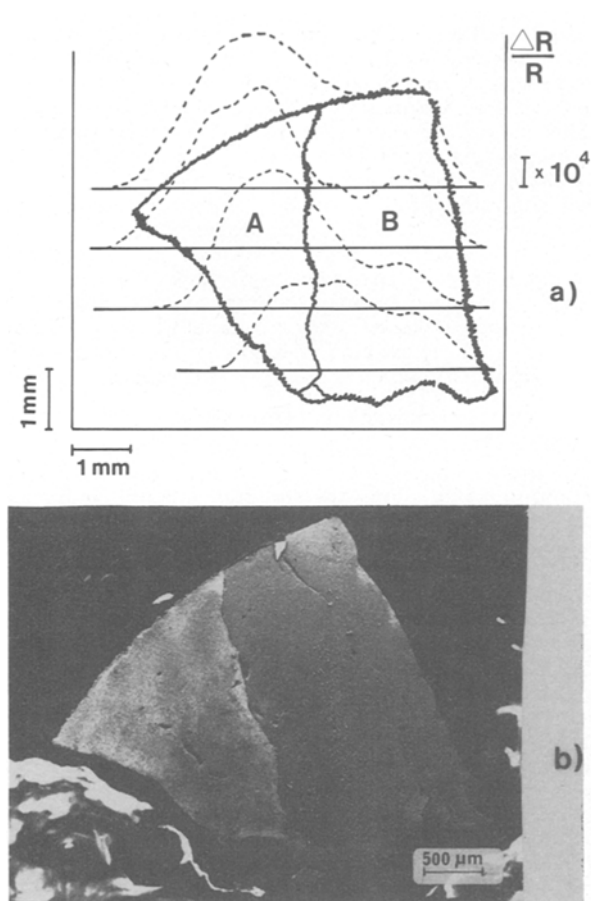


Fig. 4 (a) Map of the  $\Delta R/R$  response of the pristine surface of the  $\text{CuInSe}_2$  sample S2 in the aqueous polyiodide solution under illumination with a 1216 nm light spot ( $V_{ac} = 0.3\text{V}$  peak-to-peak,  $f = 200\text{ Hz}$ ). The electrode was dc biased at 0V vs. SCE. (b) Micrograph of the surface of the same sample S2 after lead electrodeposition at  $-0.5\text{V}$  vs. SCE for 3 min in a 1M  $\text{PbCl}_2$  aqueous solution.

part of Fig. 3b corresponding to area B of Fig. 3a. To deeper analyze these aspects, a systematic topological investigation was performed by EER after dissolution of the electrodeposited Pb in  $\text{HNO}_3$ , scanning the whole surface of the electrode with a monochromatic light spot and measuring the intensity of the  $\Delta R/R$  signal (Fig. 3a and 4a). The comparison of the EER map with the corresponding micrography clearly shows the correlation between the EER and electrochemical results. In fact, the intensity of the  $\Delta R/R$  signal is higher in the regions where lead electrodeposited and, on the contrary, is lower where electrodeposition hardly took place.

Particularly interesting is the so-called B area of sample Si (Fig. 3), that is, the extended and well-delimited region where lead electrodeposited at grain boundaries, exclusively. This area is expected to have a high resistivity.

As to sample S2, we noted that lead is electrodeposited scarcely and irregularly on the so-called B area (Fig. 4b). This seems to indicate that the electrical resistivity is low in area B, in agreement with the EER observation (Fig. 4a).

Special attention deserves the EER spectra measured on the A and B areas of sample Si polarized at 0V vs. SCE (Fig. 5). In agreement with previous results, the intensity of the  $\Delta R/R$  signal in area A is much higher than that in area B and the lineshapes differ considerably. In particular, the half-width of the EER signal in area A is much larger than that in area B. According to Aspnes theory (23), these results indicate that both area A and B are differently doped, and in particular that the former has a higher donor concentration,  $N_D$ . In fact, low-field EER spectra obtained using fully depleted space-charge regions show  $\Delta R/R$  signals directly proportional to  $N_D$  (19). Moreover, the lifetime of the charge carriers,  $\tau$ , is related to the broadening energy  $\Gamma$  (i.e., to the lifetime-induced uncertainty in the unperturbed electron energy levels) by the relationship  $\tau =$

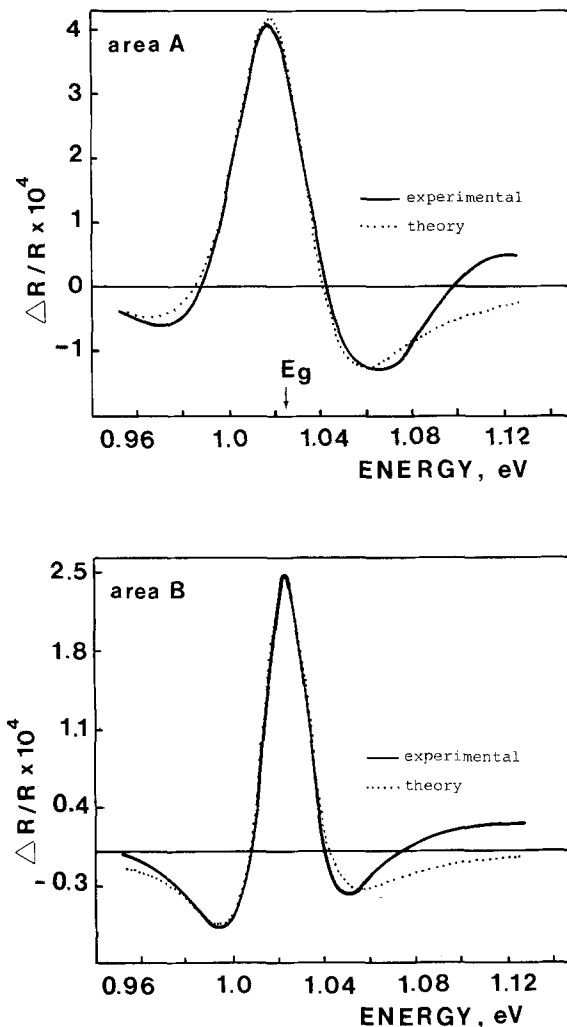


Fig. 5. Electroreflectance spectrum of area A and B of the  $\text{CuInSe}_2$  sample S1 polarized at  $V_{dc} = 0\text{V}$  vs. SCE in the aqueous polyiodide solution ( $V_{ac} = 0.3\text{V}$  peak-to-peak,  $f = 200\text{ Hz}$ ).

$\hbar/2\Gamma$  (23). So, a shorter lifetime is expected for carriers in the more heavily doped regions. In fact, by fitting the experimental curves according to Aspnes equation (23) we obtain for area A and B,  $\Gamma = 0.037$  and  $0.024\text{ eV}$ , respectively, while the phase factor,  $\theta$ , is  $203^\circ$  and  $240^\circ$ . The band-gap is equal to  $1.022\text{ eV}$ , in agreement with low temperature studies (24).

The results obtained on area A are in fair agreement with those obtained on  $\text{CuInSe}_2$  single crystals (15). The phase factor, however, differs from previous results probably owing to a different distribution in the electric field in the region of the light penetration depth due to the difference in the defects structure and concentration. The unsatisfactory fitting of the high energy tail of the experimental curve shown in Fig. 5 may be due to the presence in this region of the transition of uncertain origin, discussed by Shen *et al.* (15).

The EER technique also provides reliable measurements of the semiconductor flatband potential since the  $\Delta R/R$  signal decreases to zero and changes its sign when the semiconductor bands go from depletion to accumulation (25). Thus, we also investigated the dependence on the dc bias voltage of the EER response at a constant ac modulating voltage and wavelength (25c) as depicted in Fig. 6. Again, the two different areas of specimen S1 were considered. While the  $\Delta R/R$  response of area B decreases steeply to zero at about  $-0.1\text{V}$  vs. SCE, that of area A does not change sign until reaching much more negative potentials ( $\sim -1.2\text{V}$  vs. SCE).

We have recently shown that surface lattice defects at CdS electrodes dramatically decrease their electroreduction overpotential. Such electroreduction occurs at potentials near  $V_{FB}$  (18). A similar effect could explain the re-

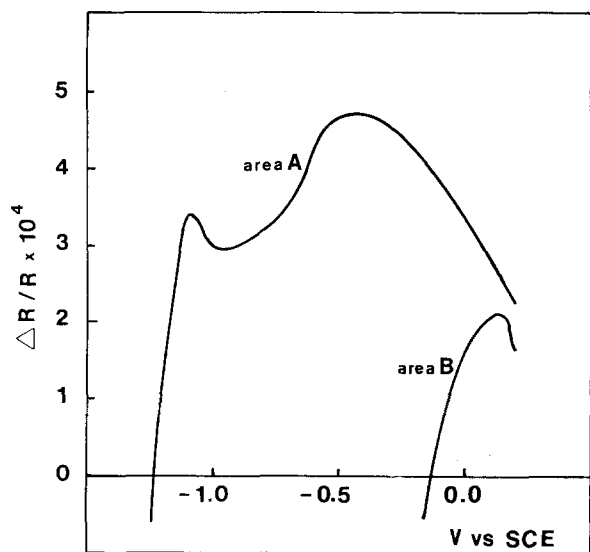
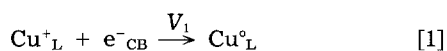
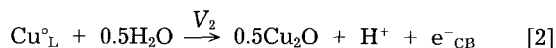


Fig. 6. Electroreflectance response at  $\lambda = 1212$  nm of area A and B of the CuInSe<sub>2</sub> sample S1 in the aqueous polyiodide solution ( $V_{ac} = 0.3$  V peak-to-peak,  $f = 200$  Hz).

sults shown in Fig. 6 (area A). In fact, the voltammogram in the dark of the CuInSe<sub>2</sub> electrode in 0.1M Na<sub>2</sub>SO<sub>3</sub> (Fig. 7a) shows a couple of well-defined peaks, a cathodic and an anodic one, at about  $-600$  mV and  $+80$  mV vs. SCE, respectively. Seemingly, the cathodic peak is associated with the irreversible electroreduction of Cu<sup>+</sup><sub>L</sub> lattice ions



while the anodic peak should correspond to Cu<sup>0</sup><sub>L</sub> stripping possibly according to the following reaction (26)



the resultant of [1] and [2] being electrode dissolution. The excess of negative charge accumulated at the CuInSe<sub>2</sub> surface during reaction [1], which begins at about  $-0.1$  V vs. SCE, causes the bands unpinning observed in Fig. 6 (curve

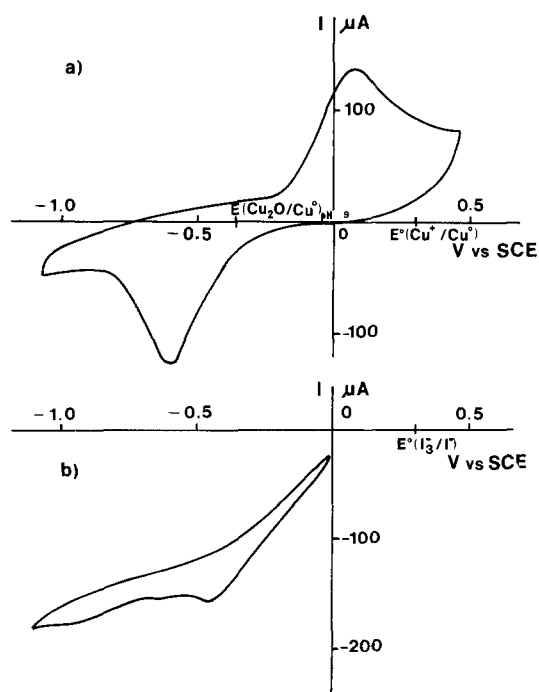
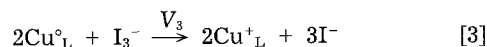


Fig. 7. Voltammograms in the dark of the CuInSe<sub>2</sub> sample S1 in: (a) 0.1M Na<sub>2</sub>SO<sub>3</sub>; (b) 2M KI + 0.01M I<sub>2</sub>. Scan rate, 100 mV/s.

A). On the other hand, as shown in the voltammogram of Fig. 7b, the electroreduction of I<sub>3</sub><sup>-</sup> takes place nearly at the same potential as reaction [1]. Therefore, a two-step mechanism may be envisaged where [1] is the first step of the I<sub>3</sub><sup>-</sup> reduction and electrons are further transferred in a second step from Cu<sup>0</sup><sub>L</sub> surface species to the I<sub>3</sub><sup>-</sup> ions, according to



If reaction [3] is the limiting step of the overall reaction (i.e.,  $V_1 \gg V_3$ ) which seems to be the case for the highly conductive area A in Fig. 6, some negative charges accumulate at the electrode surface, and  $V_{\text{FB}}$  shifts towards negative values, as inferred from the  $\Delta R/R$  vs.  $V_{\text{ac}}$  plot. By contrast, in the highly resistive area B, where lead is hardly electrodeposited,  $V_3 \gg V_1$  (i.e. reaction [1] is the limiting step) so that the electrode surface cannot be electroreduced and bands unpinning cannot be observed (Fig. 6, curve B).

Further support to this model explaining the different behavior of both area A and B is found in the photocurrent vs. potential curves obtained with hand-chopped white light (Fig. 8). The most remarkable results in this figure are (i) the anodic photocurrents in area A are about 3 times greater than those in area B, as expected from the higher donor concentration (lower electric resistivity) of area A. (ii) In area B, a photocurrent change from anodic to cathodic is observed at  $-0.1$  vs. SCE, just the potential at which the electric field at the semiconductor-electrolyte interface changes sign according to the EER measurements of Fig. 6. This is the behavior expected for a low-doped n-type semiconductor where an accumulation layer can be formed only at potentials much more negative than  $V_{\text{FB}}$ . (iii) By contrast, in the less resistive area A, with a higher  $N_{\text{D}}$ , the onset potential of the anodic photocurrent,  $V_{\text{ON}}$ , is at about  $-0.3$  V vs. SCE. Besides, a steady-state anodic photocurrent appears at potentials more negative than  $V_{\text{ON}}$ , a fact consistent with the bands unpinning ob-

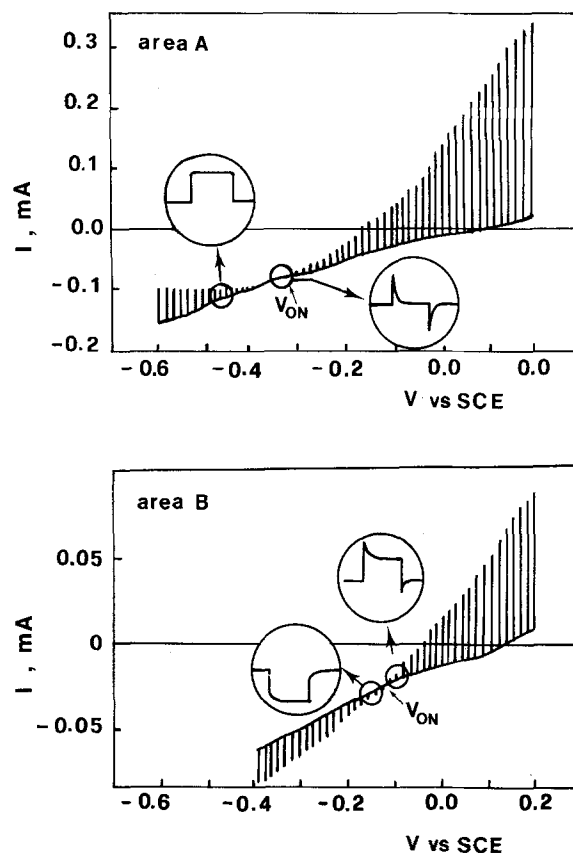


Fig. 8. Photocurrent vs. potential curves of area A and B of the CuInSe<sub>2</sub> sample S1 in the aqueous polyiodide solution measured with a hand chopped white light spot. Scan rate 5 mV/s. The insets show the photocurrent transient behavior near the onset potential,  $V_{\text{ON}}$ .

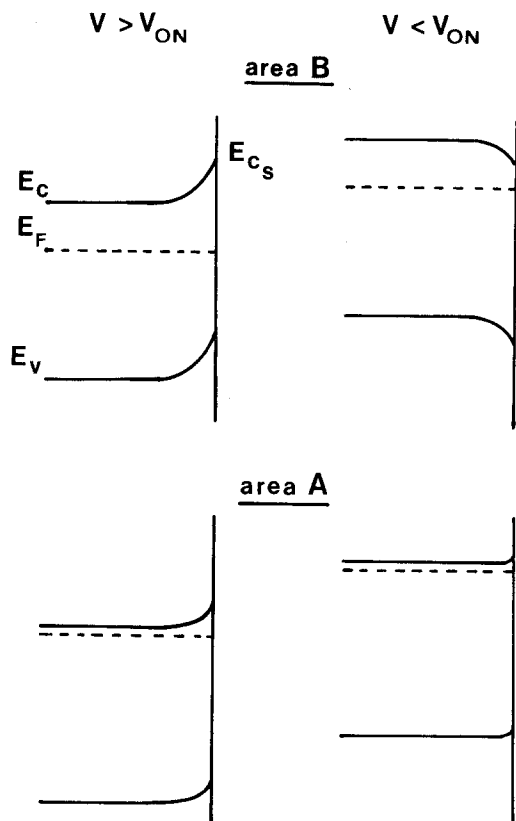


Fig. 9. Energy diagram showing the situation of the bands in area A and B of the CuInSe<sub>2</sub> sample S1 at both positive and negative potentials with respect to the photocurrent onset potential,  $V_{ON}$ .

served for this area. The energy diagrams of Fig. 9 resume the evolution of the semiconductor bands in both area A and B when polarizing the electrode from positive to negative potentials with respect to  $V_{ON}$ .

In the low-doped area B, the electric field at the semiconductor-electrolyte interface changes sign when the electrode is polarized from anodic to cathodic potentials with respect to  $V_{FB}$ , but no accumulation layer is generated. On the other hand, in the high-doped area A, the bands are unpinned because of the surface electroreduction and a nearly flatband situation is maintained at potentials much more negative than  $V_{ON}$ .

### Conclusions

The above results evidence the importance of performing EER and PEC measurements on differential surface areas by simultaneously inspecting the electrode surface by optical microscopy.

Lead electrodeposition on the CuInSe<sub>2</sub> surface is shown to mimic the EER response and to be a powerful method for visualizing semiconductor areas having different electrical resistivity. In particular, the intense lead deposition at the grain boundaries where lattice defects concentrate is illuminating.

Systematic mapping of the polycrystalline CuInSe<sub>2</sub> sample evidences that domains with a small donor concentration may exist on the surface of the low-resistive n-type semiconductor. Similar results were previously observed for single-crystal electrodes of layered transition metal dichalcogenides, such as n-WSe<sub>2</sub> (27) and n-MoSe<sub>2</sub> (28) where even p-type regions were recognized. These results are not unexpected in CuInSe<sub>2</sub>, since it was found empirically that small changes in the stoichiometry of the constituent elements can produce significant variations of carriers type and concentration (29) leading to conductivity changes by several orders of magnitude.

EER measurements on the low-resistive area show bands unpinning under polarization at potentials more cathodic than  $V_{FB}$ . This was attributed to the accumulation of negative charges on the semiconductor surface during the electroreduction of the electrode. This variation takes

place only in the zone of low resistivity where the electroreduction of metals (Pb) occurs preferentially. Apparently, surface lattice defects catalyze both kind of reactions (18, 22, 30, 31).

In order to produce efficient devices, optimization of the electrical properties of polycrystalline CuInSe<sub>2</sub> electrodes seems to be necessary. For this purpose, the control of the semiconductor surface through an *in situ* light-spot technique may be important.

### Acknowledgments

Part of this work was carried out under the auspices of the Italian-Spanish Scientific Exchange agreement. The research was supported by the Progetto Finalizzato Energetica-2, CNR-ENEA, contract CNR no. 86.00908.59 (Politecnico di Milano) and contract CNR no. 86.00942.59 (Università di Roma), and by the "Comite Conjunto Hispano-Nothamerico para la Cooperacion Cientifica y Technologica," contract no. CCA 83/038 (Instituto de Catalisis y Petroleoquimica). F. Decker would like to thank the International Centre for Theoretical Physics, Trieste (ICTP), for the support received during the stay at Italian laboratories.

Manuscript submitted Aug. 10, 1987; revised manuscript received Nov. 4, 1987.

### REFERENCES

1. Y. Mirovsky and D. Cahen, *Appl. Phys. Lett.*, **40**, 727 (1982).
2. S. Menezes, H. J. Lewerenz, and K. J. Bachmann, *Nature (London)*, **305**, 615 (1983).
3. K. J. Bachmann, S. Menezes, R. Koetz, M. Fearheily, and H. J. Lewerenz, *Surf. Sci.*, **138**, 475 (1984).
4. S. Menezes, H. J. Lewerenz, G. Betz, K. J. Bachmann, and R. Koetz, *This Journal*, **131**, 3030 (1984).
5. S. Menezes, *Appl. Phys. Lett.*, **45**, 148 (1984).
6. D. Cahen and Y. W. Chen, *ibid.*, **45**, 746 (1984).
7. D. Cahen, G. Degan, Y. Mirovsky, G. Hodes, W. Giriat, and M. Lübke, *This Journal*, **132**, 1062 (1985).
8. Y. Mirovsky, R. Tenne, D. Cahen, G. Sawatzky, and M. Polak, *ibid.*, **132**, 1070 (1985).
9. S. Menezes, *Sol. Cells, Proc. Int. Colloq.*, **16**, 255 (1986).
10. D. Cahen, Y. W. Chen, R. Noufi, R. Ahrenkiel, R. Matson, M. Tomkiewicz, and W. M. Shen, *ibid.*, **16**, 529 (1986).
11. G. Razzini, L. Peraldo Bicelli, B. Scrosati, and L. Zanotti, *This Journal*, **133**, 351 (1986).
12. G. Razzini, L. Peraldo Bicelli, M. Arfelli, and B. Scrosati, *J. Electroanal. Chem.*, **208**, 85 (1986).
13. G. Razzini, L. Peraldo Bicelli, B. Scrosati, M. Pujadas, and P. Salvador, Submitted to *This Journal*.
14. G. Razzini, *J. Power Sources*, **5**, 263 (1980); L. Peraldo Bicelli and G. Razzini, *Surf. Technol.*, **16**, 37 (1982).
15. W. M. Shen, W. Siripala, M. Tomkiewicz, and D. Cahen, *This Journal*, **133**, 107 (1986).
16. J. M. Wrobel, U. K. Reddy, L. C. Bassett, J. L. Aubel, and S. Sundaram, *J. Appl. Phys.*, **60**, 368 (1986).
17. M. Pujadas and P. Salvador, *J. Phys. Chem.*, In press.
18. I. J. Ferrer, M. Pujadas, and P. Salvador, Submitted to *Chem. Phys. Lett.*
19. F. H. Pollak, C. E. Okeke, P. E. Vanier, and P. M. Raccah, *J. Appl. Phys.*, **49**, 4216 (1978); **50**, 5375 (1979).
20. J. L. Aubel, G. Pidick, U. K. Reddy, and S. Sundaram, *Rev. Sci. Instrum.*, **56**, 268 (1985).
21. T. E. Furtak, D. C. Canfield, and B. A. Parkinson, *J. Appl. Phys.*, **51**, 6018 (1978).
22. L. Perado Bicelli and G. Razzini, *Surf. Technol.*, **20**, 393 (1983).
23. D. E. Aspnes, *Surf. Sci.*, **37**, 418 (1973).
24. J. L. Shay, B. Tell, H. M. Kasper, and L. M. Schiavone, *Phys. Rev. B.*, **7**, 4485 (1973).
25. See for instance: (a) F. M. Pollak, in "Photoelectrochemistry: Fundamental Processes and Measurement Techniques," W. L. Wallace, A. J. Nozik, S. K. Deb, and R. H. Wilson, Editors, p. 608, The Electrochemical Society Softbound Proceedings Series, Pennington, NJ (1982); (b) G. A. Scholz and H. Gerischer, *This Journal*, **132**, 1643 (1985); (c) I. J. Ferrer, H. Muraki, and P. Salvador, *J. Phys. Chem.*, **20**, 2805 (1986).
26. M. Pourbaix, "Atlas of Electrochemical Equilibria in Aqueous Solutions," 2nd ed., p. 387, NACE, Houston, TX and CEBELCOR, Brussels (1984).

27. S. Menezes, L. F. Schneemeyr, and H. J. Lewerenz, *Appl. Phys. Lett.*, **38**, 949 (1981).
28. L. Peraldo Bicelli and G. Razzini, *Surf. Technol.*, **22**, 115 (1984).
29. R. Noufi, R. Axton, C. Herrington, and S. K. Deb, *Appl. Phys. Lett.*, **45**, 668 (1984).
30. L. Fornarini and B. Scorsati, *Electrochim. Acta*, **28**, 667 (1983).
31. O. P. Bahl, E. L. Evans, and Y. M. Thomas, *Surf. Sci.*, **8**, 473 (1967).

## High-Pressure Electrochemical Oxidation of Benzene at a Lead Dioxide Electrode in Aqueous Bisulfate Solutions at 25° to 250°C

Allen J. Bard\*

*Department of Chemistry, University of Texas, Austin, Texas 78712*

William M. Flarsheim\*\* and Keith P. Johnston

*Department of Chemical Engineering, University of Texas, Austin, Texas 78712*

### ABSTRACT

The oxidation of benzene at a lead dioxide electrode which produces predominantly benzoquinone, maleic acid, and carbon dioxide, has been investigated in aqueous NaHSO<sub>4</sub> solutions as a function of temperature up to 250°C. An increase in the benzene concentration does not increase the concentration of benzoquinone formed at high temperature, which is different from the behavior at 25°C. The formation of biphenyl at high temperature was also discovered. A novel type of single-pass flow reactor for studying high temperature electrochemistry is described.

The oxidation of benzene to benzoquinone at a lead dioxide electrode in aqueous sulfate solutions is limited by the low solubility of benzene in water. Clarke *et al.* have determined a reaction order with respect to benzene of 2 (1). Benzene solubility in water increases significantly with increasing temperature; the two fluids become miscible at 297°C at a pressure of 243 bar (2). This study examines the effect of increasing temperature and increasing benzene concentration on the electrochemical oxidation of benzene on lead dioxide in the temperature range 25°-250°C.

Supercritical water has a combination of low dielectric constant and high dipole moment that make it useful for a number of novel chemical applications. Water has a dipole moment of 1.84 debye, and at ambient conditions it is extensively hydrogen bonded. This gives rise to a high dielectric constant, 78 at 25°C, making water an excellent solvent for ions and a poor one for nonpolar species. High temperature disrupts the hydrogen bonding and correlated orientation of water molecules (3) and decreases the density and thereby lowers the dielectric constant to 5.2 at the critical point (374°C, 221 bar) (4). Because of the low dielectric constant, water in the critical region is an excellent solvent for organic molecules. The water dipoles still orient in the vicinity of an ion, however, and produce a locally high dielectric constant, so strong electrolytes remain dissolved and dissociated in supercritical water. The simultaneous solvation of both polar and nonpolar molecules makes supercritical water a powerful solvent. The MODAR process takes advantage of this superior solvent power in using supercritical water as a reaction medium for the destructive oxidation of organic waste (5). Other workers have investigated the use of supercritical water at milder conditions to clean and liquify coal (6), and to hydrolyze plant material into useful fuels (7).

In a previous paper, we described electroanalytical measurements made in supercritical water at temperatures up to 390°C (8). An electrochemical cell was developed to operate at the extreme temperature and pressure of supercritical water. In addition, the voltammetric behavior of water, KBr, KI, and hydroquinone was studied, and the diffusion coefficients of I<sup>-</sup> and hydroquinone were measured. Building on this experimental back-

ground, the present work is an expansion into the area of high-temperature electro-organic synthesis, specifically benzene oxidation. In supercritical water, high concentrations of nonpolar materials can be combined with strong electrolytes in a one-phase system, and this presents the possibility of synthetic routes that are not hindered by mass transfer across a phase boundary. Although temperatures above 250°C are not reported here, the apparatus and experimental procedures described could be used up to 375°C with only minor modification.

The electrochemical oxidation of benzene was first studied near the end of the last century (9) and has been discussed frequently in the literature (1, 10-14). Work through 1976 has been summarized by Clarke *et al.* (1). The desired product from the oxidation is benzoquinone, which can then be reduced to hydroquinone. Hydroquinone is used as an anti-oxidant in the manufacture of rubber and other products. Other major products from the oxidation are maleic acid and carbon dioxide.

The specific overall electrode reactions involved in oxidizing benzene are shown in Fig. 1. The complete conversion of benzene to carbon dioxide requires the removal of 30 electrons and the participation of 12 water molecules. This full oxidation can occur readily at a platinum electrode (15). Lead dioxide is the only reported electrode material that produces large quantities of benzoquinone or maleic acid. A lead dioxide electrode will perform the first stage oxidation to benzoquinone readily in acidic sulfate media; however, the yield and current efficiency vary greatly depending on the specific conditions of electrolysis. As the concentration of benzoquinone builds in the solution, the benzoquinone is usually oxidized further to maleic acid, accompanied by two moles of carbon dioxide. Clarke *et al.* (1) report that at very low over-voltage, the benzoquinone is not oxidized further. The one-step oxidation of benzene to maleic acid was studied extensively by Ito *et al.* (13). This pathway is important under most reaction conditions. Few previous workers analyzed the carbon dioxide generated during oxidation, and no one has discussed the pathway by which it is formed. This study shows that single-step oxidation of benzene to carbon dioxide can occur on lead dioxide, especially at high temperature. (The term single-step is used here to mean that once benzoquinone or maleic acid is formed and desorbed

\*Electrochemical Society Active Member.

\*\*Electrochemical Society Student Member.